Journal of Colloid and Interface Science 709 (2026) 139925

Contents lists available at ScienceDirect

Journal of Colloid And Interface Science

journal homepage: www.elsevier.com/locate/jcis

Etching-assisted fabrication of photonic microparticles with tunable dual and quadruple stopbands from mono-sized and binary silica colloidal particles

Penghui Li [a], Jiawei Wu [a], Kaijun Chen [a], Anxin Shang [a], Jiakun Dong [a], Yuandu Hu [a,b,c,d,e,*]

[a] Department of Materials Science and Engineering, School of Physical Science and Engineering, Beijing Jiaotong University, Beijing 100044, China
[b] Hubei Key Laboatory of Plasma Chemistry and Advanced Materials, Wuhan Institute of Technology, Wuhan 430205, China
[c] Hubei Provincial Key Laboratory of Green Materials for Light Industry, Hubei University of Technology, Wuhan 430068, China
[d] Guangdong Provincial Key Laboratory of Technique and Equipment for Macromolecular Advanced Manufacturing, South China University of Technology, Guangzhou 510641, China
[e] Key Laboratory of Advanced Materials of Ministry of Education, Tsinghua University, Beijing 100084, China

GRAPHICAL ABSTRACT

A strategy to generate dual and quadruple stopbands photonic microparticles from mono-sized and binary SiO_2 colloidal particles through controllable etching has been proposed. The resultant photonic microparticles can be used to construct photonic patterns with tunable wettability.

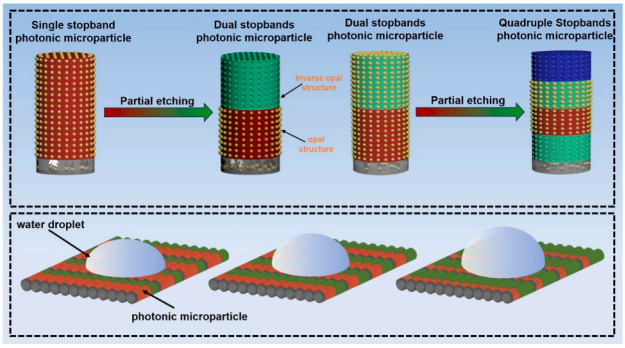

ARTICLE INFO

Keywords:
Photonic microparticle
Dual-stopband
Selective etching
Anti-counterfeiting
Antifouling

ABSTRACT

The integration of multiple photonic stopbands into a single microparticle is a coveted goal for advancing multiplexed sensing and high-capacity information encryption. However, conventional fabrication methods typically rely on the complex integration of different colloidal building blocks in terms of sizes or compositions, which increases cost and limits scalability. Herein, we report a facile and scalable strategy for fabricating cylindrical photonic microparticles with tunable dual stopbands from a single photonic composition, thereby eliminating the reliance on different colloidal building blocks. Our approach synergistically combines micromolding with a magnetic field-assisted selective etching process. The incorporation of ferromagnetic barium ferrite nanoparticles ($BaFe_{12}O_{19}$ NPs) enables precise orientation control of the microparticles, which is pivotal for the site-specific protection and etching that integrates both opal and inverse opal structures into a single

* Corresponding author at: Department of Materials Science and Engineering, School of Physical Science and Engineering, Beijing Jiaotong University, Beijing 100044, China.
E-mail address: huyd@bjtu.edu.cn (Y. Hu).

https://doi.org/10.1016/j.jcis.2026.139925
Received 8 December 2025; Received in revised form 9 January 2026; Accepted 16 January 2026
Available online 17 January 2026

microparticle. The ratio between these two distinct photonic regions can be readily tuned, allowing for customizable photonic properties and structural colors. Furthermore, we demonstrate the extensibility of this method by creating multi-segment photonic microparticles with more than two stopbands. Due to the different wettability between the opal and inverse opal regions, the microparticle array exhibits adjustable hydrophilicity and hydrophobicity and potentially possesses antifouling capability. These programmable microparticles, with their anisotropic and tunable optical characteristics, together with tunable hydrophobicity, offer significant potential for developing next-generation information encoding platforms, anti-counterfeiting technologies and displays, and even antifouling pigments.

1. Introduction

Photonic crystals are an ordered structure formed by the periodic alternating arrangement of two or more materials with different dielectric constants in space [1–4]. Periodic nanostructures develop structural colors through the reflection of selected wavelengths of visible light. Structural colors have the advantages of fade resistance and eco-friendliness, demonstrating promising potential in fields such as pigments, sensors, displays, and anti-counterfeiting [5–18]. In nature, many organisms exploit complex photonic nanostructures to produce multiple structural colors for camouflage, communication, and warning [19–25]. Inspired by these biological systems, the integration of multiple photonic stopbands into a single artificial microparticle has emerged as a powerful strategy for enhancing the functionality of photonic crystals, particularly for multiplexed sensing and high-capacity information encryption.

To date, several methods have been developed to fabricate individual photonic microparticle with multiple stopbands [26–33]. A common strategy involves the assembly of multiple types of colloidal building blocks with different sizes within confined geometries, such as microfluidic droplets. For instance, Kim et al. fabricated dual-stopband Janus microspheres using a two-channel microfluidic device by injecting photocurable resin (ETPTA) suspensions containing SiO_2 colloidal particles (CPs) of different diameters [26]. Similarly, multiple structural colors were achieved by injecting photonic suspensions containing SiO_2 CPs with different sizes. Zhao et al. prepared spherical and rod-like multiple stopbands photonic barcodes with core-shell structures using a multi-channel microfluidic device [29]. Yang et al. successfully fabricated photonic microcapsules with dual and triple stopbands by manipulating the interaction among polystyrene (PS) CPs with different sizes within double-emulsion droplets through depletion force [34]. Flow lithography and stepwise lithography were employed by Kim et al. to fabricate columnar and disc-shaped photonic microparticles, respectively [35,36]. By utilizing different photonic suspensions, distinct structural colors were achieved in each geometry. The discontinuous multistep process results in low production efficiency for traditional photolithography. Although flow lithography is a continuous process, it requires a low Reynolds number and complex setup and precise control to integrate multiple stopbands onto a single particle. Overall, these approaches inherently rely on the precise synthesis and handling of multiple building blocks, which increases experimental complexity and cost. An attractive alternative is to generate multiple stopbands from a single photonic composition. In a previous study, we demonstrated the feasibility of this concept by preparing bullet-like dual-stopband microparticles from a single photonic suspension via a selective etching technique [37]. However, broader application of this elegant approach is limited by challenges in achieving precise and scalable control over the orientation of the microparticles during the selective etching process, which is crucial for defining the stopband patterns.

Herein, we report a controllable and scalable strategy for fabricating photonic microparticles with tunable dual stopbands from a single photonic composition. Our method involves micromolding followed by a selective etching process. We successfully prepared cylindrical photonic microparticles with a single stopband, which consist of monodisperse SiO_2 colloidal particles (CPs) and resin, using micromolding technology. The incorporation of ferromagnetic barium ferrite nanoparticles ($BaFe_{12}O_{19}$ NPs) allows for precise orientation control of the microparticles, enabling the site-specific etching required to integrate both opal and inverse opal structures onto a single microparticle. The ratio between these two distinct photonic regions can be readily tuned, allowing for customization of the optical properties. Furthermore, we demonstrate the extension of this method to create multi-segment microparticles with more than dual stopbands. Photonic microparticle arrays with varying wettability were prepared by utilizing microparticles with different structures. These programmable photonic microparticles, with their anisotropic and tunable optical characteristics, exhibit significant potential for advanced applications in digital encoding, anti-counterfeiting technologies and display, and even antifouling pigment.

2. Experimental section

2.1. Materials

Aqueous ammonia ($NH_3{\cdot}H_2O$, ≥28%), ethanol (≥99.7%), tetraethyl orthosilicate (TEOS, electronic grade), hydrofluoric acid (HF), and polystyrene (PS, Mw ~ 350 k) were purchased from Aladdin Co., Ltd. Ethoxylated trimethylolpropane triacrylate (ETPTA, ≥99%) and dichloromethane (CH_2Cl_2, ≥99.5%) were ordered from Sigma-Aldrich Co., Ltd. 2-Hydroxy-2-methyl propiophenone (photoinitiator 1173, >96.0%) was purchased from TiXi Ai HuaCheng Industry Development Co., Ltd. Barium ferrite nanoparticles ($BaFe_{12}O_{19}$ NPs, average diameter of 80 nm, M_w: 1111.46 g/mol) were purchased from ZhongNuo Advanced Material Technology Co., Ltd. All the reagents were used as received.

2.2. Synthesis of SiO_2 CPs

The SiO_2 CPs were synthesized by the Stöber method [38]. Initially, 8 mL of $NH_3{\cdot}H_2O$, 3 mL of deionized water, and ethanol were added to a conical flask. Then, 6 mL of TEOS was added and stirred at 60 °C with a rate of 500 rpm for the sol-gel process for 2 h. The product was centrifuged at 6000 rpm for 10 min and washed with ethanol. The purified SiO_2 CPs were dispersed in ethanol for further use. Different sizes of SiO_2 CPs can be obtained by changing the amount of ethanol (Fig. S1).

2.3. Preparation of ETPTA suspension of SiO_2 CPs

The suspension of SiO_2 CPs in ethanol was mixed with ETPTA resin containing 1% *w/*w photoinitiator 1173 at a certain volume fraction. Ethanol evaporated from the mixture at 70 °C to achieve the viscous suspension with a specific structural color. Photonic suspension with distinct structural colors was achieved using SiO_2 CPs with different sizes.

2.4. Preparation of cylindrical photonic microparticles and photonic films

The SiO_2-ETPTA suspension was dropped onto a PDMS mold with an array (10 * 10) of cylindrical holes with a diameter of 400 μm and a depth of 1.2 mm (Fig. S2). The holes were filled with the suspension under vacuum. After removing excess photonic suspension, the whole

mold was irradiated with a UV lamp (Gabon ZF-5, 16 W, Shanghai, China) to polymerize the ETPTA. Finally, the cylindrical photonic microparticles were separated from the mold. To prepare magnetic cylindrical photonic microparticles, ethanol was added to the photonic suspension. The mold is incubated at 70 °C in a convection oven for 15 min to evaporate ethanol, resulting in the partial occupancy of each individual hole, where the final filled height was determined by the volume fraction of the nonvolatile solvent in the suspension. To make a magneto-responsive compartment, 6% w/w $BaFe_{12}O_{19}$ NPs were dispersed in ETPTA. The SiO_2 CPs of 307 nm were additionally dispersed in ETPTA at a volume fraction of 0.12. After filling the hole arrays in the mold with magnetic suspension and residual suspension was removed, the mold was placed between two neodymium magnets for 3 min to align the $BaFe_{12}O_{19}$ NPs; the mold was then irradiated with UV. Finally, magneto-responsive cylindrical photonic microparticles were obtained.

To prepare the SiO_2/ETPTA photonic film, a red photonic suspension was added to the mold and irradiated with a UV lamp to polymerize ETPTA. Finally, the film was separated from the mold. The obtained photonic film was further conducted HF etching and transformed into an inverse opal photonic film with green structural color.

2.5. Partial etching reaction for the fabrication cylindrical dual-stopband photonic microparticles

The cylindrical photonic microparticles, containing magneto-responsive compartments, were vertically aligned in a custom container (10 mm × 10 mm × 1.5 mm) under an external magnetic field. A controlled volume of water was fed to partially immerse the microparticle arrays from the bottom, followed by freezing at −20 °C. Following this, PS solution in CH_2Cl_2 (40 mg/mL) was dispensed into the container from the top, fully encapsulating the cylinder arrays. Upon solvent evaporation, a PS film was formed, embedding the arrays (Fig. S3). The PS-encapsulated microparticle arrays were removed from liquid water and carefully immersed in a 10% HF solution for 1–3 min to selectively etch the SiO_2 CP. The photonic microparticles were separated and washed with water. When an appropriate amount of CH_2Cl_2 solution of PS was used, the middle part of the photonic microparticle arrays can be effectively protected, therefore allowing for selective etching at both exposed ends.

2.6. Fluorescence functionalization of cylindrical dual-stopband photonic microparticles

To impart fluorescence, the photonic microparticles were incubated at 35 °C for 12 h in an aqueous solution of ruthenium-functionalized polymer (pNIPAAm-*co*-Ru(bpy)₃). PNIPAAm-*co*-Ru(bpy)$_3$ copolymers were synthesized by free radical polymerization [39].

2.7. Characterizations

The sizes of SiO_2 CPs were investigated by transmission electron microscopy (TEM, JEOL, JEM-1400, Japan). An optical microscope (Olympus Corporation, Olympus BX53M, China) was used to record the photonic microparticles under different modes of reflection and transmission. Reflection spectra were collected by an Olympus microscope (reflection mode) equipped with a fiber optic spectrometer (USB Flame-S, Ocean Insight, Inc., China). Morphologies of the photonic microparticles were characterized by scanning electron microscope (SEM, Hitachi S-4800, Japan).

3. Results and discussion

SiO_2 CPs dispersed in the photocurable resin ETPTA form a solvation layer on their surface. This is due to hydrogen bonding between surface silanol groups and the acrylate groups of the resin [40]. When the SiO_2 CPs reach a certain volume fraction, the interparticle repulsion causes the SiO_2 CPs to spontaneously organize into a crystalline structure with a face-centered cubic (FCC) lattice structure [41–43]. This periodic structure endows the suspensions with vivid iridescent colors (Fig. S4). To fabricate cylindrical photonic microparticles, the ETPTA photocurable suspension of SiO_2 CPs was molded using a PDMS mold featuring a 10 × 10 array of cylindrical holes (diameter: 400 μm; height: 1.2 mm) (Fig. 1a). The photocurable suspension was dropped onto the PDMS mold to completely fill the holes under vacuum. The excess suspension was then removed, and the filled mold was irradiated with UV light to polymerize the resin suspension in the hole arrays. Finally, the cylindrical photonic microparticles were separated from the mold. Here, cylindrical photonic microparticles with different structural colors (red, green, and blue) were obtained by using SiO_2 CPs with diameters of 206 nm, 176 nm, and 160 nm, respectively (Fig. 1b–d). Their photographs in petri dishes and corresponding reflection spectra are shown in Fig. 1e–g. To demonstrate the integration of dual-stopband structures, the initial red photonic microparticles were selected as an example. The as-prepared cylindrical microparticles were first adhered to a polyimide double-sided tape to ensure vertical orientation. A controlled volume of water was then added to partially immerse the arrayed microparticles, followed by solidification at −20 °C. Subsequently, a certain amount of PS solution in CH_2Cl_2 was fed to completely fill the array. After the CH_2Cl_2 evaporated, the upper part of the array was embedded and protected by a PS film. The PS-protected array was then removed after the ice was melted and immersed in an HF solution for selective etching. Following the etching of the SiO_2 CPs, an inverse opal structure was generated on the surface, thereby achieving a dual-stopband structure (Figs. S5 and S6). However, this method requires the initial fixation of microparticles with double-sided tape, which complicates the process and limits its efficiency for upscale production. Therefore, developing a more robust and widely applicable method for controlling microparticles' orientation during selective etching is the key objective for our following investigation.

Herein, directed manipulation of photonic microparticles was achieved by incorporating magnetic components. The preparation process for the magneto-responsive cylindrical photonic microparticles is illustrated in Fig. 2a. First, SiO_2-ETPTA suspension diluted with ethanol (~12.5 vol%) was dropped onto a PDMS mold. The mold's hole arrays were filled with the suspension under vacuum. After the ethanol was evaporated at 70 °C, each individual hole arrays was partially occupied by the photonic suspension. The photonic layer was then cured by UV irradiation, creating a gap above it. A suspension of magnetic nanoparticles was introduced to fill this gap. The height of the photonic layer can be controlled by adjusting the initial volume of ethanol. The magnetic layer was prepared from an ETPTA suspension containing 5% w/w $BaFe_{12}O_{19}$ NPs (D = 80 nm) and SiO_2 CPs (D = 307 nm, Φ = 0.12). The $BaFe_{12}O_{19}$ NPs are ferromagnetic and exhibit high stability against corrosion, retaining their magnetic properties even after HF treatment [44]. The addition of SiO_2 CPs increased the suspension's viscosity, thereby preventing severe agglomeration of the $BaFe_{12}O_{19}$ NPs. After the remaining part of the hole arrays was filled with the magnetic suspension, the mold was placed between a pair of magnets to align the $BaFe_{12}O_{19}$ NPs along the external magnetic field. Subsequently, UV irradiation fixed the aligned NPs in the polymerized matrix, endowing the magnetic layer with a net magnetic moment. Finally, the photonic microparticles were separated from the mold. Optical microscopy images of the prepared red magneto-responsive cylindrical photonic microparticles are shown in Fig. 2b–c, and it exhibits angle-independent photonic property (Fig. S7). The orientation of these microparticles can be controlled by an external magnetic field. For instance, when the magnetic field direction was perpendicular to the substrate plane, the microparticles stood upright (Figs. S8 and S9). Furthermore, both surface and cross-sectional SEM images reveal the SiO_2 CPs were assembled into the FCC (1 0 0) plane, rather than the typical (1 1 1) plane (Fig. 2d–f, Figs. S10 and S11) [45].

Leveraging their magnetic responsiveness, the cylindrical photonic

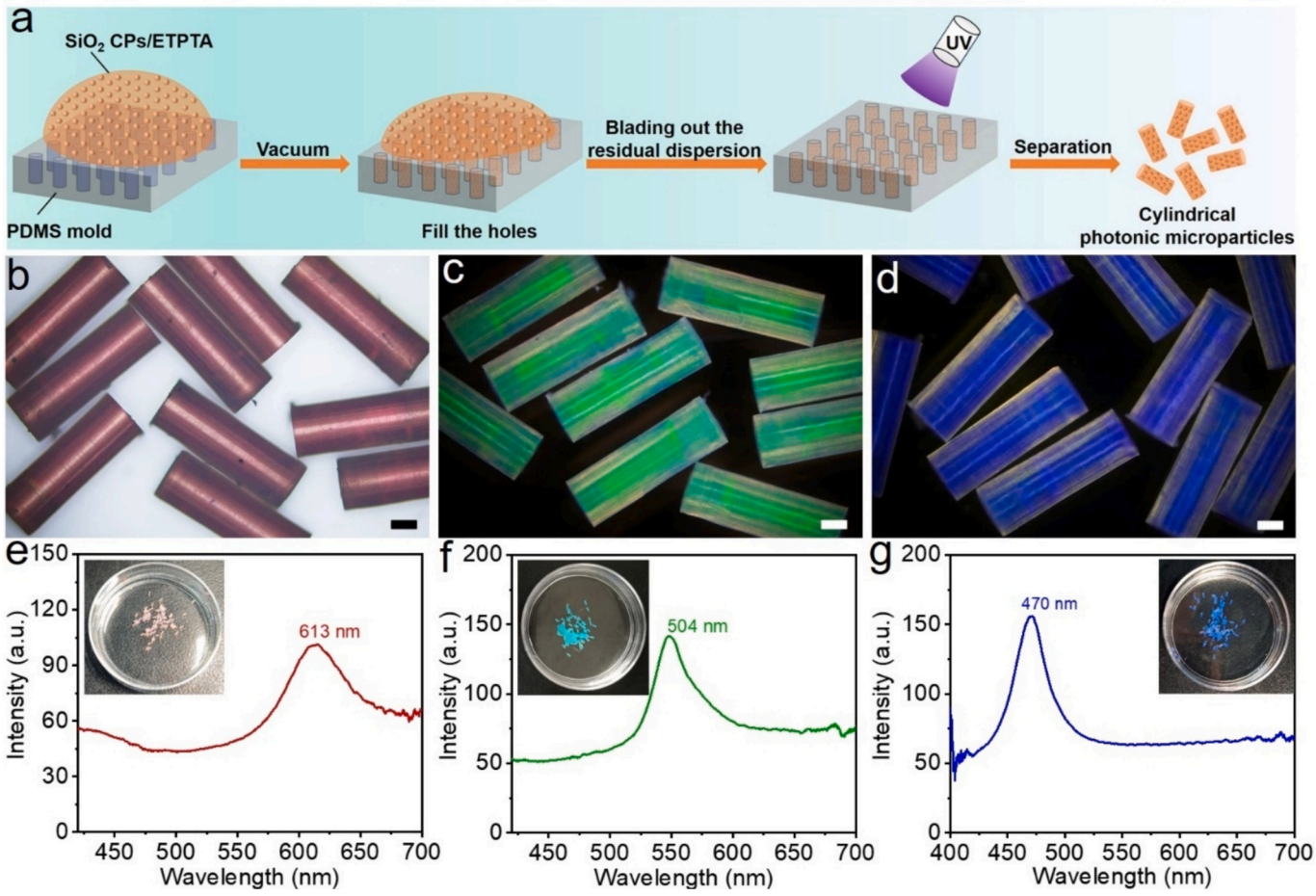

Fig. 1. (a) Schematic diagram illustrating the fabrication procedure of cylindrical photonic microparticles. Optical microscopy images of red, green, and blue cylindrical photonic microparticles (b–d) and their reflection spectra (e–g), respectively. Inset figures in e–g are their corresponding photographs in petri dishes. The scale bars are all 200 μm. (For interpretation of the references to color in this figure legend, the reader is referred to the web version of this article.)

microparticles were oriented upright in grooves under an external magnetic field. The selective etching method described previously was then applied (Fig. 3a), and allowing us to successfully integrate both opal and inverse opal structures within a single microparticle. The initial red microparticles were transformed into microparticles with partial red and partial green (Fig. 3b–c). After the removal of the SiO_2 CPs, the original reflective peak blue-shifted and broadened due to the increased refractive index contrast in the inverse opal region. The resultant photonic microparticles thus exhibited two distinct reflection peaks at 570 and 608 nm (Fig. 3d). SEM images confirmed the presence of macropores in the etched region (Fig. 3f, g and Fig. S12), while no such pores were found in the protected part, with a clear boundary visible between the two regions. In the case of the FCC (1 0 0) planes, d is half the lattice constant (a), so the volume fraction can be expressed as [46]:

$$\phi = \frac{2D^3\pi}{3a^3} = \frac{D^3\pi}{12d^3} \tag{1}$$

The maximum reflection spectra of the photonic microparticles follows the Bragg diffraction equation:

$$\lambda = 2dn_{eff} = \left(\frac{2\pi}{3\phi}\right)^{\frac{1}{3}} D\left(n_{silica}^2\phi + n_{pETPTA}^2(1-\phi)\right)^{\frac{1}{2}} \tag{2}$$

where n_{eff} is the effective refractive index of the photonic microparticle. ϕ represents the volume fraction of the SiO_2 CP. n_{silica} and n_{pETPTA} are the refractive indices of the SiO_2 CP (1.45) and pETPTA matrix material (1.47). D=206 nm, ϕ=0.26. The λ value was calculated at 605 nm. After the etching process, the n_{eff} of the etched region is the synergy of porous polymerized ETPTA (pETPTA) resin and air (n_{air} = 1). The calculated λ was 563 nm, which was close to the experimental result. Fig. 3h illustrates the transformation of the initial cylindrical photonic microparticle with a single stopband into dual stopbands. Furthermore, by changing the direction of the magnetic field during the protection step, the magnetic end can be protected, therefore enabling the fabrication of cylindrical dual-stopband photonic microparticles with different patterns through etching (Fig. S13). For the etching process, the etching became slower from the initial rate of ~5.0 μm/min to ~0.82 μm/min with the etching depth (Fig. S14a–b). It is worth mentioning that the etching depth doesn't affect the optical properties of the photonic microparticle (Fig. S14c). This protection was not only effective on the surface but also effectively slowed the diffusion of HF into the interior of the protected area (Fig. S15).

The selective etching method exhibits great flexibility. The surface ratio of the opal to inverse-opal structure on the cylindrical photonic microparticle can be readily tuned by varying the initial amount of water added. Given that the size of the groove is 10 mm * 10 mm * 1.5 mm, the linear relationship between the initial aqueous solution volume and the etched surface area of the microparticle can be established and shown in Fig. 4a. In this process, PS protected the unetched region. Consequently, a small amount of the water fed leads to a small portion of the inverse opal structure on the final dual-stopband photonic microparticle. For example, when 35 μL, 55 μL, 75 μL, and 90 μL of aqueous solution were added, the etched surface areas were approximately 0.54 mm^2, 0.81 mm^2, 1.13 mm^2, and 1.28 mm^2, respectively. The resultant cylindrical dual-stopband photonic microparticles are shown in Fig. 4b.

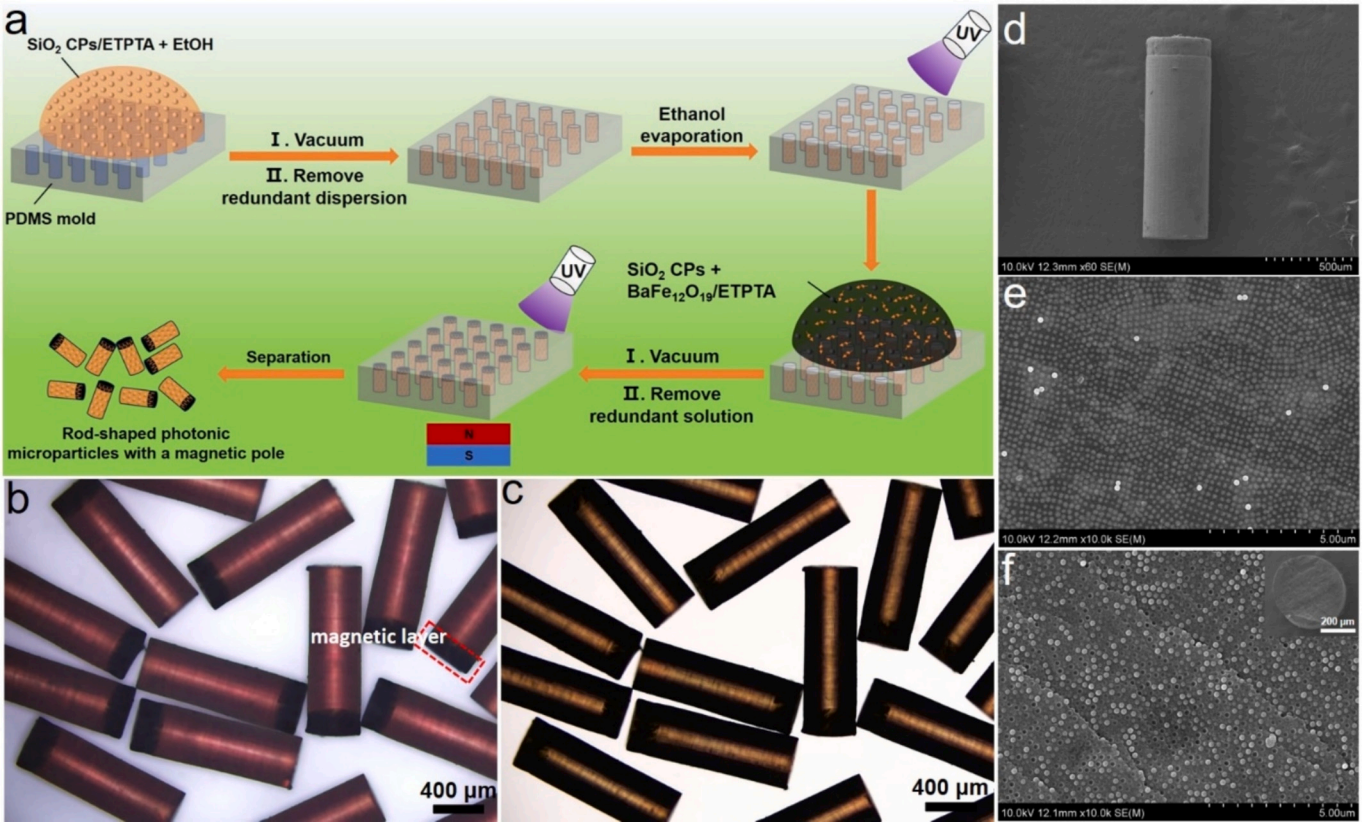

Fig. 2. (a) Schematic diagram illustrating the fabrication procedure of the magneto-responsive cylindrical photonic microparticles. Optical microscopy images (b, reflection mode and c, transmission mode) of the magnetic NPs-loaded cylindrical photonic microparticles. (d–f) SEM images of the cylindrical photonic microparticle, the surface, and the cross section of the microparticle.

Alternatively, control of the structures can be achieved by adjusting the volume of the CH_2Cl_2 solution of PS. When the solution was insufficient to cover the whole upper region of the array, the middle part of the microparticles was protected. Fig. S16a shows the linear relationship between the volume of the CH_2Cl_2 solution of PS and the unetched surface area. By fixing the water volume at 25 μL and varying the volume of CH_2Cl_2 solution of PS, a series of dual-stopband photonic microparticles were obtained (Fig. S16b). Therefore, this simple and controllable protection strategy provides a convenient avenue for generating a family of cylindrical dual-stopband photonic microparticles, which are featured with diverse structures and tunable stopband characteristics.

Dual-stopband photonic microparticles were successfully prepared from a single photonic suspension. Furthermore, we fabricated dual-stopband microparticles by sequentially molding two photonic suspensions with different structural colors (Fig. 5a–b). Building on this concept, photonic microparticles with three and four stopbands were also created through the selective etching process, as shown in Fig. S17 and Fig. 5c–d, respectively. The resultant photonic microparticles thus exhibited four distinct reflection peaks (Fig. 5e). Fig. 5f illustrates the process of generating the multiple stopbands structure.

The tunable ratio of the opal to inverse opal portion on the microparticle surface holds significant potential for information encoding. As a proof of concept, a cylindrical photonic microparticle with an etched-to-protected ratio of 1/4 was assigned the digital code "1" (Fig. S18a). These encoded microparticles can be integrated into larger-scale architectures, such as for cards (Fig. S18b). Additional encryption can be achieved by introducing fluorescent substances into the inverse-opal regions, thereby enabling a combination of structural color and fluorescence signatures (Fig. S19a) [47]. In addition, the structural color and reflection spectra of the photonic microparticle are less influenced by filling the ruthenium polymer, which is important for information anti-counterfeiting (Fig. S19b). Concurrently, information can be hidden by setting distinct magnetic moment directions in microparticles with identical etching ratios (Fig. S20). Ultimately, a triple anti-counterfeiting system consisting of structural color visualization, fluorescence, and magnetic response verification can be formed. In conclusion, these photonic microparticles represent a promising platform for advanced digital coding applications.

In addition, the unetched opal region, composed of polymer and SiO_2 CPs is hydrophilic given the presence of a large amount of uncovered surface of the SiO_2 CPs. In contrast, the inverse opal region formed from etching features a porous polymer skeleton, which exhibits relatively less hydrophilic due to the increased roughness (Fig. S21). By precisely controlling the etching area ratio of the microparticle, these two distinct wetting characteristics can be integrated into planar patterns of photonic microparticles at the millimeter scale, therefore enabling the patterns with tunable hydrophilic-hydrophobic properties. For example, when the patterns used the unetched rod-like photonic microparticles, the etched photonic microparticles with different degrees of etching from 1/3 to 2/3, and the fully etched photonic microparticles, the contact angles of water droplets varied from 56°, 64°, 74°, 81°, and 90° (Fig. 6, Figs. S22, and S23). It is worthy of mentioning that the contact angle of the surface based on the etched microparticle array is higher than that of the etched photonic film. This was likely due to the presence of hierarchy structure for the microparticle arrays, while the etched film is a relatively flat surface. Specifically, the pattern from microparticle arrays possesses a porous-on-a curved surface, while the photonic film only possesses a porous flat surface (as illustrated in Fig. S24). The contact angle variations in the contact angles have a special meaning for the patterns. Specifically, when the individual particle with a higher etched-to-unetched ratio was used as building block for contructing an

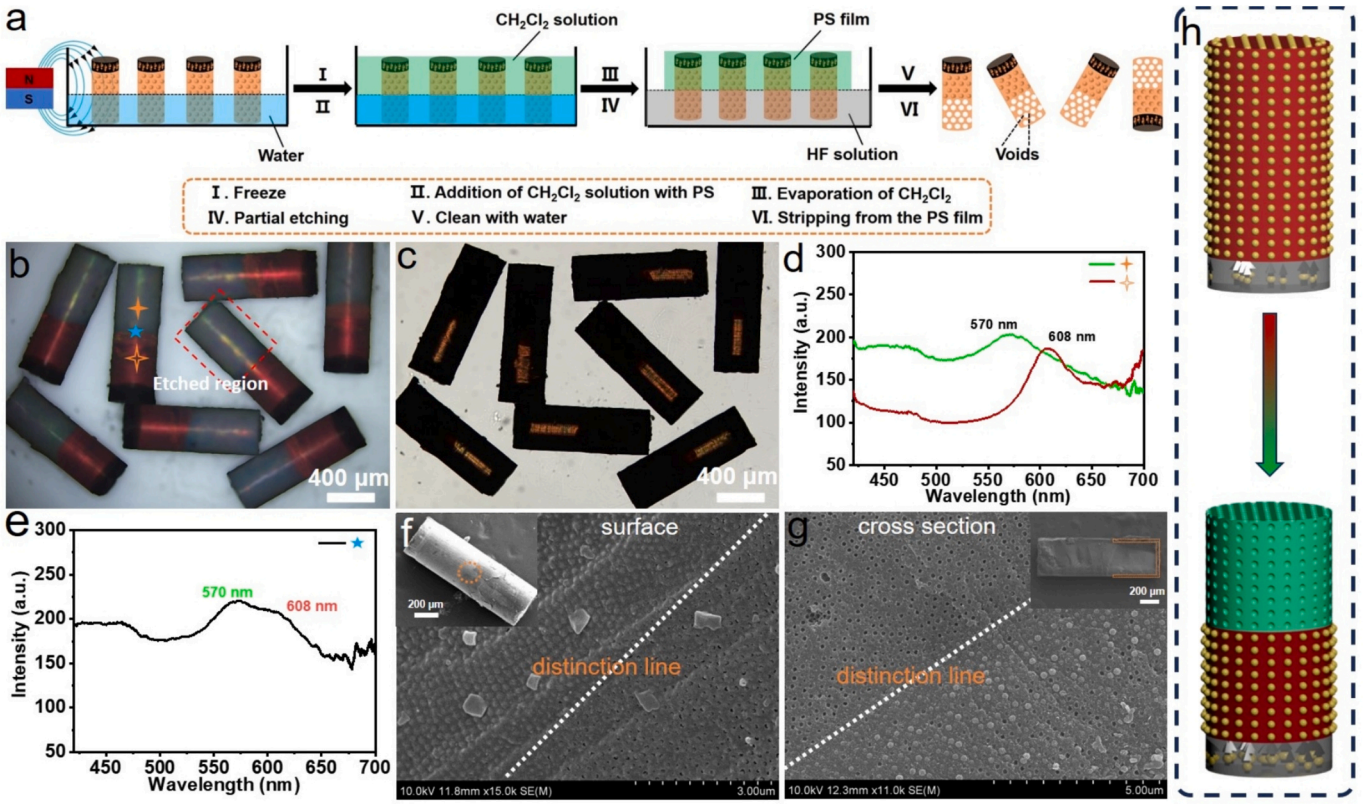

Fig. 3. (a) Schematic fabrication of the dual-stopband photonic microparticles via protection-assisted etching. Optical microscopy images (b. reflection mode, and c. transmission mode) of the cylindrical dual-stopband photonic microparticles. (d–e) Reflection spectra of the cylindrical dual-stopband photonic microparticle. SEM images of the surface (f) and cross-section (g) of the partially etched photonic microparticle. (h) Schematic structure of the cylindrical photonic microparticle before and after etching.

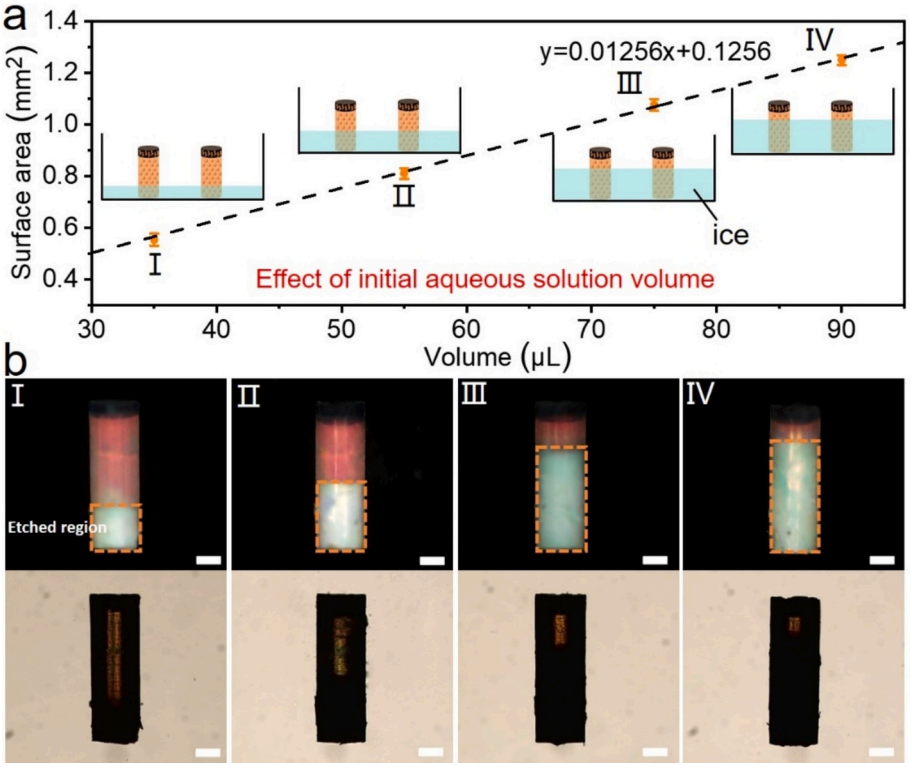

Fig. 4. (a) The relationship between the volume of aqueous solution in the groove and the surface etched area of the microparticle. The line is the theoretical value, and the point is the actual value. (b) Optical microscopy images (reflection mode (upper row) and transmission mode (bottom row)) of the cylindrical dual-stopband photonic microparticle with varied etching degrees. The scale bars are all 200 μm.

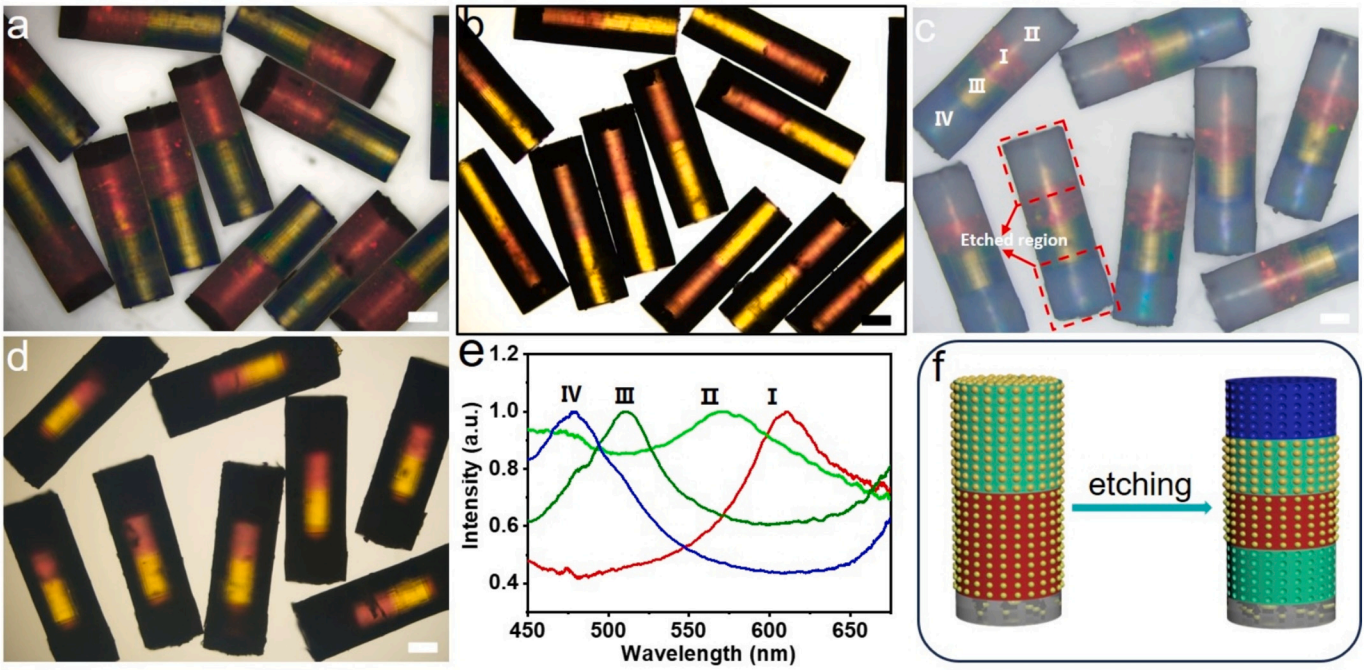

Fig. 5. Optical microscopy images (reflection/transmission mode) of several cylindrical dual-stopband photonic microparticles before (a, b) and after (c, d) etching. The scale bars are all 200 μm. (e) Reflection spectra of the cylindrical quadruple stopband photonic microparticle formed from the etching of dual-stopband photonic microparticle. (f) Schematic structure of the cylindrical dual-stopband photonic microparticle before and after etching.

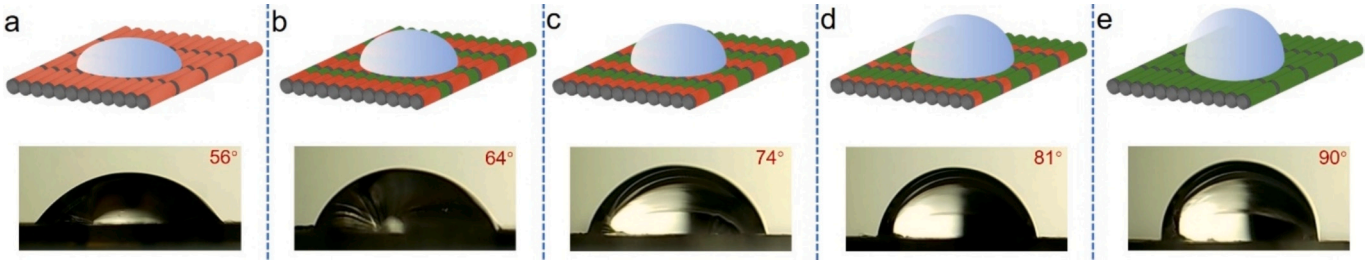

Fig. 6. Schematic diagram and corresponding contact angle photos of water droplet on the patterns of photonic microparticle layer. The red and green parts represent opal region and inverse opal region, respectively. (For interpretation of the references to color in this figure legend, the reader is referred to the web version of this article.)

anti-counterfeiting label or color pattern, under simple water rinsing, water droplets can more easily roll off and carry away surface contaminants than that of patterns formed from the photonic particles with a lower etched-to-unetched ratio, thereby achieving a self-cleaning effect. This helps prevent irreversible contamination damage and may remarkablely extend the pattern's service life. The individual photonic microparticle with partially etched structure not only can provide multiple structural colors for the patterns but can also potentially enhance the antifouling properties of the patterns.

4. Conclusions

In conclusion, we have developed a facile and highly controllable approach for the fabrication of cylindrical photonic microparticles with tunable dual stopbands. By leveraging a single photonic suspension and a combination of micromolding and selective etching processes, we have successfully integrated both opal and inverse opal structures on an individual photonic microparticle. The incorporation of $BaFe_{12}O_{19}$ NPs enabled magnetic alignment, significantly enhancing the process's controllability and scalability compared to previous physical fixation methods. The ratio between the two regions was precisely adjustable by varying the volume of solutions, allowing for the creation of a family of microparticles with customized photonic properties. Furthermore, the strong flexibility of our method was evidenced by its successful extension to fabricate multi-segment photonic microparticles with more than two stopbands. More importantly, a sophisticated triple anti-counterfeiting system was conceptualized, integrating structural color patterns, fluorescence, and magnetic response verification. Based on the structural differences between opal and inverse opal regions, photonic microparticle arrays with tunable wettability was also constructed. Moreover, the array formed from etched photonic microparticles demonstrated enhanced hydrophobicity than that of the resin-based inverse opal photonic film. These photonic microparticles, with their anisotropic and tunable optical characteristics, exhibit substantial potential for developing next-generation platforms in high-security information encoding, antifouling pigments, advanced anti-counterfeiting labels, and miniaturized integrated photonics.

CRediT authorship contribution statement

Penghui Li: Writing – original draft, Visualization, Validation, Methodology, Investigation, Data curation. **Jiawei Wu:** Methodology, Investigation. **Kaijun Chen:** Methodology, Investigation. **Anxin Shang:** Investigation. **Jiakun Dong:** Methodology, Investigation. **Yuandu Hu:**

Writing – review & editing, Supervision, Resources, Project administration, Funding acquisition, Conceptualization.

Declaration of competing interest

The authors declare that they have no known competing financial interests or personal relationships that could have appeared to influence the work reported in this paper.

Acknowledgments

This work is supported by the Fundamental Research Funds for the Central Universities (No. 2025JBZX005 (Y. H.), No. 2024YJS195 (P. L.)). Y. H. is grateful for the open research funds from the Guangdong Provincial Key Laboratory of Technique and Equipment for Macromolecular Advanced Manufacturing (No. 20240518), the open research fund from Hubei Provincial Key Laboratory of Green Materials for Light Industry, Hubei University of Technology (No. 202409B01), and Fund of Key Laboratory of Advanced Materials of Ministry of Education, Tsinghua University (No. Advmat-2402).

Appendix A. Supplementary data

Supplementary data to this article can be found online at https://doi.org/10.1016/j.jcis.2026.139925.

Data availability

Data will be made available on request.

References

[1] E. Yablonovitch, Inhibited spontaneous emission in solid-state physics and electronics, Phys. Rev. Lett. 58 (1987) 2059–2062.
[2] S. John, Strong localization of photons in certain disordered dielectric superlattices, Phys. Rev. Lett. 58 (1987) 2486–2489.
[3] Z. Cai, Z. Li, S. Ravaine, M. He, Y. Song, Y. Yin, H. Zheng, J. Teng, A. Zhang, From colloidal particles to photonic crystals: advances in self-assembly and their emerging applications, Chem. Soc. Rev. 50 (2021) 5898–5951.
[4] Q. He, H. Vijayamohanan, J. Li, T.M. Swager, Multifunctional photonic Janus particles, J. Am. Chem. Soc. 144 (2022) 5661–5667.
[5] J.H. Holtz, S.A. Asher, Polymerized colloidal crystal hydrogel films as intelligent chemical sensing materials, Nature 389 (1997) 829–832.
[6] J. Wang, T. Yin, J. Ge, A disposable thermally triggered photonic crystal anti-counterfeiting tag with irreversible response and multi-step color changes, Small 20 (2024) 2311308.
[7] S. Wu, J. Nan, Y. Wu, Z. Meng, S. Zhang, Low-angle-dependent anticounterfeiting label decoded by alcohol tissue wiping based on a multilayer photonic crystal structure, ACS Appl. Mater. Interfaces 14 (2022) 27048–27055.
[8] N. Li, L. Cai, M. Lu, F. Bian, W. Sun, Y. Zhao, Prickly Janus magnetic and photonic microrobots for exosome assays, Chem. Eng. J. 494 (2024) 153085.
[9] G. Li, X. Qu, L. Hao, Q. Li, S. Chen, A microfluidics-dispensing-printing strategy for Janus photonic crystal microspheres towards smart patterned displays, J. Polym. Sci. 60 (2022) 1710–1717.
[10] E.S.A. Goerlitzer, R.N.K. Taylor, N. Vogel, Bioinspired photonic pigments from colloidal self-assembly, Adv. Mater. 30 (2018) 1706654.
[11] X. Du, S. Zhang, J. Zhou, H. Chi, Z. Sheng, Y. Hu, C. Shang, T. Wang, G. Chen, Z. Yang, Inverse opal torus-shaped photonic microobjects with superior stimulus-responsive properties to their spherical equivalents, Small 21 (2025) 2412117.
[12] Y. Wu, Y. Wang, S.F. Zhang, S.L. Wu, Artificial chameleon skin with super-sensitive thermal and mechanochromic response, ACS Nano 15 (2021) 15720–15729.
[13] T. Hueckel, G.M. Hocky, J. Palacci, S. Sacanna, Ionic solids from common colloids, Nature 580 (2020) 487–490.
[14] S. Yin, S. Yang, C. Wang, S. Chen, Magnetic-directed assembly from Janus building blocks to multiplex molecular-analogue photonic crystal structures, J. Am. Chem. Soc. 138 (2016) 566–573.
[15] H. Wang, L. Cai, D. Zhang, L. Shang, Y. Zhao, Responsive Janus structural color hydrogel micromotors for label-free multiplex assays, Research 2021 (2021) 9829068.
[16] Y. Fang, W. Fei, X. Shen, J. Guo, C. Wang, Magneto-sensitive photonic crystal ink for quick printing of smart devices with structural colors, Mater. Horiz. 8 (2021) 2079–2087.
[17] K. Chen, Q. Fu, S. Ye, J. Ge, Multicolor printing using electric-field-responsive and photocurable photonic crystals, Adv. Funct. Mater. 27 (2017) 1702825.
[18] Y. Hu, Z. Tian, D. Ma, C. Qi, D. Yang, S. Huang, Smart colloidal photonic crystal sensors, Adv. Colloid Interface Sci. 324 (2024) 103089.
[19] S. Yoshioka, S. Kinoshita, Wavelength-selective and anisotropic light-diffusing scale on the wing of the morpho butterfly, Proc. R. Soc. B 271 (2004) 581–587.
[20] J. Han, H. Su, F. Song, J. Gu, D. Zhang, L. Hang, Novel photonic crystals: incorporation of nano-CdS into the natural photonic crystals within peacock feathers, Langmuir 25 (2009) 3207–3211.
[21] J. Sun, B. Bhushan, J. Tong, Structural coloration in nature, RSC Adv. 3 (2013) 14862–14889.
[22] M. Kuang, J. Wang, L. Jiang, Bio-inspired photonic crystals with superwettability, Chem. Soc. Rev. 45 (2016) 6833–6854.
[23] P. Vukusic, J.R. Sambles, C.R. Lawrence, Structural colour mixing in wing scales of a butterfly, Nature 404 (2000) 457.
[24] T.D. Schultz, G.D. Bernard, Pointillistic mixing of interference colors in cryptic tiger beetles, Nature 337 (1989) 72–73.
[25] G. Bogdanov, A.A. Strzelecka, N. Kaimal, S.L. Senft, S. Lee, R.T. Hanlon, A. A. Gorodetsky, Gradient refractive indices enable squid structural color and inspire multispectral materials, Science 388 (2025) 1389–1395.
[26] S.H. Kim, S.J. Jeon, G.-R. Yi, C.J. Heo, J.H. Choi, S.M. Yang, Optofluidic assembly of colloidal photonic crystals with controlled sizes, shapes, and structures, Adv. Mater. 20 (2008) 1649–1655.
[27] S. Liu, C. Wang, X. Wang, J. Zhang, Y. Tian, S. Yin, S. Chen, Tunable Janus colloidal photonic crystal supraballs with dual photonic band gaps, J. Mater. Chem. C 2 (2014) 9431–9438.
[28] M. Xiao, J. Liu, Z. Chen, W. Liu, C. Zhang, Y. Yu, C. Li, L. He, Magnetic assembly and manipulation of Janus photonic crystal supraparticles from a colloidal mixture of spheres and ellipsoids, J. Mater. Chem. C 9 (2021) 11788–11793.
[29] Y. Zhao, Z. Xie, H. Gu, L. Jin, X. Zhao, B. Wang, Z. Gu, Multifunctional photonic crystal barcodes from microfluidics, NPG Asia Mater. 4 (2012) e25.
[30] P. Li, J. Wu, K. Chen, J. Dong, Y. Hu, Advances in the fabrication of multiple stopband photonic crystal microparticles, CrystEngComm 27 (2025) 4796–4809.
[31] Q. Guo, Y. Li, Q. Liu, Y. Li, D. Song, Janus photonic microspheres with bridged lamellar structures via droplet-confined block copolymer co-assembly, Angew. Chem. Int. Ed. 61 (2022) e202113759.
[32] Y. Zhao, H. Gu, Z. Xie, H.C. Shum, B. Wang, Z. Gu, Bioinspired multifunctional Janus particles for droplet manipulation, J. Am. Chem. Soc. 135 (2013) 54–57.
[33] J.H. Lee, G.H. Choi, K.J. Park, D. Kim, J. Park, S. Lee, H. Yi, P.J. Yoo, Dual-colour generation from layered colloidal photonic crystals harnessing "core hatching" in double emulsions, J. Mater. Chem. C 7 (2019) 6924–6931.
[34] S. Yang, Y.G. Kim, S. Park, S.H. Kim, Structural color mixing in microcapsules through exclusive crystallization of binary and ternary colloids, Adv. Mater. 35 (2023) 2302750.
[35] J.Y. Sim, G.H. Lee, S.H. Kim, Microfluidic design of magnetoresponsive photonic microcylinders with multicompartments, Small 11 (2015) 4938–4945.
[36] H.S. Lee, J.H. Kim, J.S. Lee, J.Y. Sim, J.Y. Seo, Y.K. Oh, S.M. Yang, S.H. Kim, Magnetoresponsive discoidal photonic crystals toward active color pigments, Adv. Mater. 26 (2014) 5801–5807.
[37] P. Li, Y. Hu, Z. Yang, Anisotropic photonic microobjects with dual stopbands formed from single photonic dispersion and their application for anticounterfeiting, ACS Appl. Mater. Interfaces 17 (2025) 15969–15977.
[38] W. Stöber, E. Bohn, Controlled growth of monodisperse silica spheres in the micron size range, J. Colloid Interface Sci. 26 (1968) 62–69.
[39] Y. Hu, J. Tresback, J. Pérez-Mercader, Preparation of ruthenium-functionalized microgels through the intermolecular crosslinking of two functionalized polymers within droplets and study of their chemical/ photo-active behaviors, Polym. Degrad. Stab. 181 (2020) 109345.
[40] S.H. Kim, S.J. Jeon, W.C. Jeong, H.S. Park, S.M. Yang, Optofluidic synthesis of electroresponsive photonic Janus balls with isotropic structural colors, Adv. Mater. 20 (2008) 4129–4134.
[41] S.K. Nam, J.B. Kim, S.H. Han, S.H. Kim, Photonic Janus balls with controlled magnetic moment and density asymmetry, ACS Nano 14 (2020) 15714–15722.
[42] Y. Hu, A. Ardekani, J. Zhu, Y. Yang, J. Perez-Mercader, Droplet microfluidics, colloidal assembly and nanoscale processing: synergistic control and properties of colloid-based photonic microobjects, Adv. Colloid Interface Sci. 344 (2025) 103601.
[43] P. Jiang, M.J. McFarland, Large-scale fabrication of wafer-size colloidal crystals, macroporous polymers and nanocomposites by spin-coating, J. Am. Chem. Soc. 126 (2004) 13778–13786.
[44] P. Xu, X. Han, M. Wang, Synthesis and magnetic properties of $BaFe_{12}O_{19}$ hexaferrite nanoparticles by a reverse microemulsion technique, J. Phys. Chem. C 111 (2007) 5866–5870.
[45] C. Li, Y. Yu, H. Li, H. Lin, H. Cui, Y. Pan, R. Zhang, Y. Song, H.C. Shum, Heterogeneous self-assembly of a single type of nanoparticle modulated by skin formation, ACS Nano 17 (2023) 11645–11654.
[46] S.H. Nah, J.B. Kim, H.N.T. Chui, Y. Suh, S. Yang, Enhanced colorimetric detection of volatile organic compounds using a dye-incorporated photonic crystal-based sensor array, Adv. Mater. 36 (2024) 2409297.
[47] P. Li, H. Pang, Y. Zheng, Q. Cui, C. Shang, Y. Xiao, T. Hui, Y. Hu, Composite photonic microobjects with anisotropic photonic properties from a controlled wet etching approach, Colloids Surf. A Physicochem. Eng. Asp. 688 (2024) 133618.